Nanoscale

Accepted Manuscript

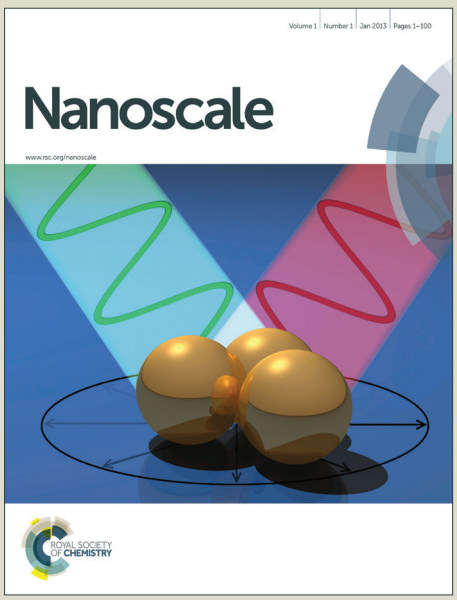

ROYAL SOCIETY OF CHEMISTRY

www.rsc.org/nanoscale

Nanoscale

RSCPublishing

ARTICLE

A Tactile Sensor Translating Texture and Sliding Motion Information into Electrical Pulses ‡

Cite this: DOI: 10.1039/xoxxoooooox

Zhipeng Liao, [a] Weihua Liu, [*a] You Wu, [a] Chen Zhang, [a] Yan Zhang, [b,c] Xiaoli Wang, [a] Xin Li [a]

Received ooth January 2012,
Accepted ooth January 2012

DOI: 10.1039/xoxxoooooox

www.rsc.org/

An electric pulse output by a nanogenerator upon a strain-and-release event resembles a neural impulse. Cutaneous receptors imbedded in skin transduce mechanical forces impinging the skin into neural impulses and the tactile information is encoded into the firing rates of the neural impulses. Here, we report a nanogenerator-type tactile sensor, which records the texture and sliding motion by outputting sequence of electric pulses. The sensitive component of the device is an NG embedded in a polydimethylsiloxane package. An artificial finger-print serving as a strain introducer mimicking finger print is integrated over the NG. The electric pulses outputted by the device transmit the texture and sliding motion information. The device demonstrates a capability of detecting punch holes with depth less than 200 μm on a nonwoven cloth. It also shows a perfect reproducibility of the electric pulses as it scans the same area of a band wire and a piece of nonwoven cloth. The artificial finger-print is the key in transferring the strain direction, which allows the active sensor (a nanogenerator) beneath to detect the bumpy structure during a touch and sliding motion.

Introduction

Nanogenerators (NGs) for mechanical energy harvesting have been demonstrating its great potential in building self-powered systems and active sensors in last decade.[1] The general physical process for energy conversion of NGs can be summarized as: charge generation, charge separation and charge flow.[2] This physical process can be accomplished by either piezoelectric effect or triboelectric effect, which presents different type of NG. Though through different physics effect, these two types of NGs share a common feature of electric output: electric pulses. Those electric pulses can be used for energy harvesting purposes.[3] It can also be collected as signal for sensing purposes.[2, 4] Cutaneous receptors imbedded in skin transduce mechanical information into neural impulses.[5] NG resembles tactile neuron of human skin in one way: they both output pulsed signal actively when trigged by deformation strain or sliding motion.

Most of the on studying artificial electronic skins (e-skins) are based on pressure image capturing strategy, which is different from human skin, for tactile sensation. To capture a pressure image, an e-skin usually comprise array of pressure sensors on a flexible substrate. The pressure-sensitive components in e-skin can be a pressure-sensitive capacitor,[6] resistor,[7] or a layer of piezoelectric material.[8] When semiconductors such as ZnO and GaN, which have piezoelectric effect, are utilized, it enables diverse of innovative device designs due to the piezotronic effect and piezophotonic effect.[9] Most recently, a tactile sensor based on piezotronic effect[10] and another one based on piezophotonic effect[11] have been demonstrated. These two devices have shown great advantages in pressure image capturing. For example, the tactile sensor based on piezotronic effect eliminated the requirement of field-effect transistors (FETs) as active matrix, which presents one of the major obstacles towards an e-skin.[10] While the tactile sensor based on piezophotonic effect can display the pressure distribution directly in a luminescent image with spatial resolution down to 2.7 μm.[11] To obtain detailed pressure image is an all-in-one solution for tactile sensation for most applications. In some specific applications, a household robot for example, the main task of an artificial electronic skin is to help the robot to judge the texture feature and sense the sliding motion of the object being in contact. For human skin, the texture and sliding motion perception is mainly based on the response of cutaneous receptors to the vibration of finger-prints.[12] In fact, a fingertip gives keenest texture recognition when it sliding on an object. A tactile sensor in some ways mimicking human skins would be applauded.

In this paper, we report a NG-type tactile sensor, which actively outputs electric pulses in responding to the surface texture during a sliding motion. Flexible dome and bumpy structures are effective mechanical transducer structure and have been adopted in developing tactile sensors.[8a, 13] To record the texture and sliding motion by NG through recording its output electric pulses, an artificial finger-print is designed as effective mechanical transducer, which can effectively cooperate with NG.

An NG, which is a piezoelectric one here for instance, is packaged in polydimethylsiloxane (PDMS) mimicking cutaneous receptors. An artificial finger-print is assembled on the NG mimicking finger-print. As the artificial finger-print been pressed and released, the pressure will be introduced to the NG beneath. The NG outputs electric pulses in response to

the press-and-release evens. The width, the amplitude as well as the polarity of the pulses conveys the tactile information.

A pressure image capturing device provides detailed texture information with spatial resolution in 2 dimensions. It usually comprises an array of pressure sensors to record the pressure from an object at different sites. Theoretically, a pressure image capturing device can provide the most detailed tactile information as we may need. The creativity of this work is that we integrated an artificial finger print with previous nanowire device. The artificial finger print can change the strain direction of external pressure. A nanogenerator is adapted as an active sensor to capture its vibration during a touch and sliding motion. By doing this, the texture and sliding motion information will be translate into sequence of electric pulses. Because the spatial distribution is transferred into time domain, it doesn't need large number of tactile pixels. The active signal output is another advantage of the device. It don't need power input from the driven circuit and so it will simplify the driven circuit. The unique feature and the advantage of the device might be valuable for the community of sensor technology.

The physical mechanism of the device reported here is also different from the other tactile sensors based on nanowires. For example, Wu's device[10] is based on piezotronic effect, whereas the piezopotential introduced by the strain modulates the Schottky barrier heights between the metal and ZnO nanowire and so changes the current goes through the wire. Pan's device[11] is based on piezophotonic effect, whereas the strain introduced inner-crystal piezopotential modulates the charge separation, transport and/or recombination in optoelectronic processes and so the light-emitting density. However, the sensitive component of the NG-type tactile sensor reported here is essentially a nanogenerator, where the strain introduced piezopotential drives charges back and forth in the external circuit. The NG-type tactile sensor could be a complement technique in the family of nanowire-based tactile sensor for applications where detailed pressure image is not asked.

Experimental

Device fabrication

The polyimide film with laminated copper foil is a commercial product. The thickness of the polyimide film is 100 μm. The copper foil is patterned with standard lithograph process with etching agent $FeCl_3$ solution. The Indium/Tin layer was fabricated by standard thermal evaporating and lift-off process. The ZnO piezoelectric fine wire (PFW) was manually assembled. The ZnO PFWs were synthesized by a physical vapour deposition method. The first layer of polydimethylsiloxane (PDMS) was spin coated at 500 rpm to cover the ZnO PFW. After the first layer of PDMS was cured, the second layer of PDMS was spin coated at 500 rpm. Then the copper wire was assembled and embedded into the second layer of PDMS. Finally, the second layer of PDMS was cured at room temperature for 24 hours.

Characterization

Measurement of the NG-type tactile sensor: The current was amplified by a low-noise current preamplifier (Stanford Research SR570) before it was recorded by a Tektronix TDS3014B digital phosphor oscilloscope. Computer-controlled motorized positioning platform (Newport model ESP301) was used to program the motion of the device.

Results and discussion

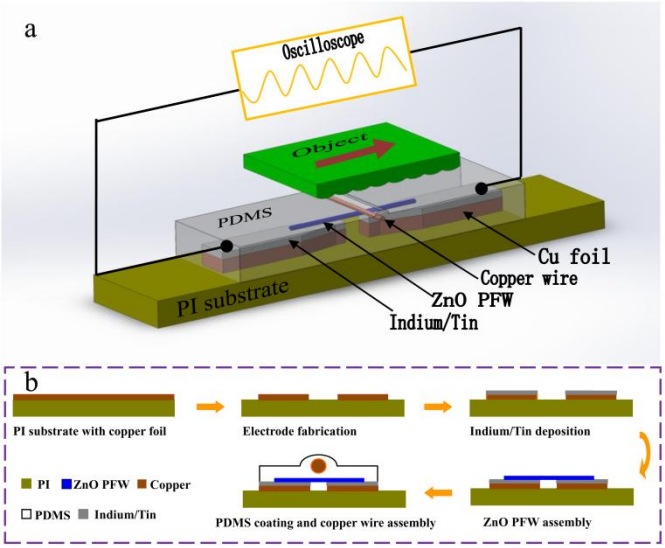

Figure 1. Schematic device design and fabrication procedures. (a) Device design and diagram of the testing approach. (b) Schematic diagram depicting the fabrication process for the NG-type tactile sensor.

A ZnO PFW (~5 μm in diameter and several hundred microns in length) is bridging between two copper electrodes so it allows free bending (Figure 1a). An artificial finger-print is formed by integrating a fine copper wire (350 μm in diameter) cross over the ZnO PFW in the PDMS package. The artificial finger-print serves as a strain introducer mimicking human finger prints. This artificial finger-print vibrates as it touching a textured surface and the mechanical vibration is transferred to the NG beneath. The NG outputs electric pulses upon the mechanical vibration. The output electric pulses are correlated to the texture and the sliding motion of the objects been touched. The fabrication process is depicted in Figure 1b. The device is fabricated on a polyimide (PI) film with a layer of laminated copper foil. The copper foil is patterned into a pair of Cu electrodes. Then a layer of alloy of Indium and Tin is selectively deposited onto the Cu electrodes. After the assembling of the ZnO PFW, the Indium and Tin is heated up to melting point to grasp the ZnO PFW. The artificial finger-print is formed by assembling a fine Cu wire across the bridging ZnO PFW in the PDMS packaging layer. The Cu wire is insulated from the ZnO PFW by a thin layer of PDMS. A metal core increases the Young's modulus of the composite structure of the artificial finger-print and so makes it more effective in transfer the mechanical vibration to the ZnO PFW beneath.

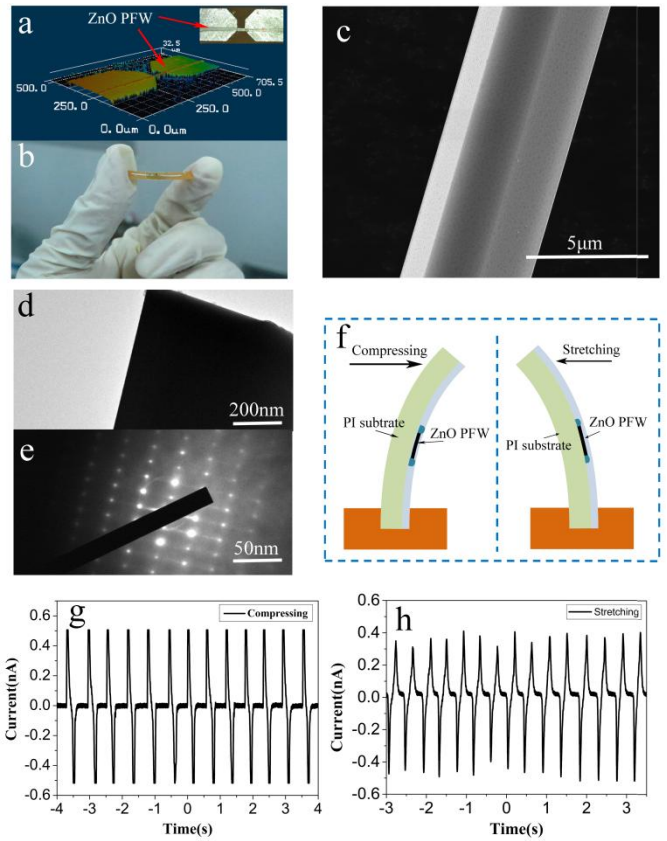

Figure 2. Device images and the contact quality test. (a) A three-dimension image of the device pre PDMS packaging and copper wire assembling. Inset figure is an optical microscope image of the device pre PDMS packaging and copper wire assembling. (b) An optical photograph of a fully fabricated NG-type tactile sensor. (c) The scanning electronic microscopy image of a ZnO PFW. (d) The transmission electron microscopy and (e) the selected area electron diffraction (SAED) pattern. (f) Diagram of the test of the device working as horizontal aligned NG (HANG). The output electric pulses of the device as it is (g) compressed-and-released and (h) stretched-and-released.

The 3-dimension (3D) optical microscopy image of the device is shown in Figure 2a. The inset figure is an optical microscope image of the device pre Cu wire assembling. The electrode gap is about 80 μm. The thickness of the Cu electrodes is about 20 microns, which defines the depth of the gap between the electrodes. The gap allows the bridging ZnO PFW bend down regardless the PI substrate bending status. Figure 2b shows a photo of the fully fabricated device. Figure 2c is a scanning electronic microscopy image of a ZnO PFW. The diameter of the ZnO PFW is about 5 μm. The transmission electron microscopy and the selected area electron diffraction (SAED) pattern are shown in Figure 2d and e, respectively. The SAED pattern shows a single crystal feature with C crystal orientation in its longitudinal axis.

During a texture detecting operation, the device will be subjected to hush scratches as it sliding on an object. A reliable contact between the ZnO PFW and the electrode is very important for the function of the device. The layer of alloy of Indium and Tin served as a grasping layer for the ZnO PFW. The reliability of the contact is verified by hundred times of bending during a test of the device as it working as a horizontal aligned NG (HANG).[14] Figure 2f is a schematic of the test. When the device is bent to left side or right side, the ZnO PFW is stretched or compressed respectively. Figure 2g and h show the test results. The device shows a typical HANG characteristic. The piezoelectric pulse polarization switched as the bent direction switches. The device output stably and is able to be operated continuously after hundreds of operation cycles.

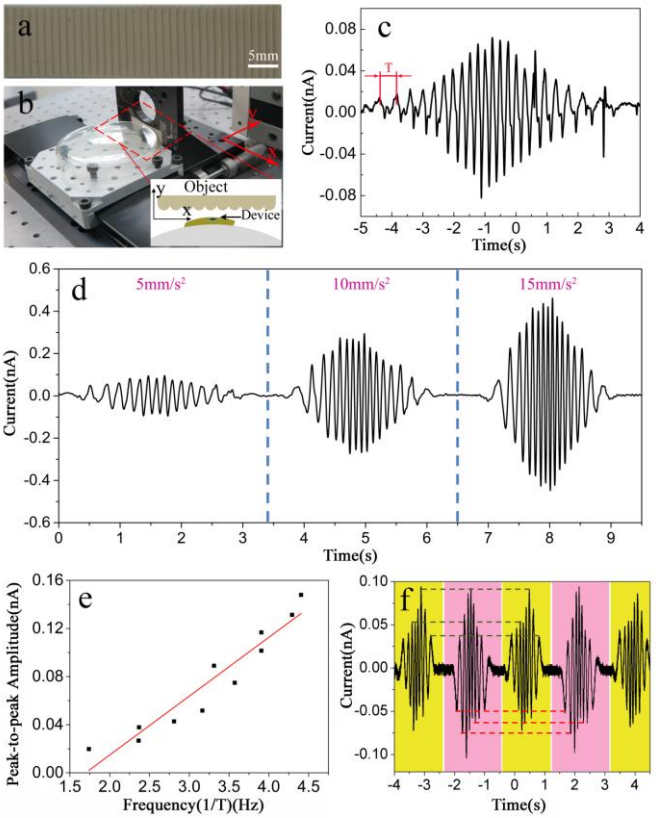

Figure 3. Responses of a NG-type tactile sensor to the bumpy structure of a ribbon wire. Photograph of (a) the ribbon wire and (b) the experimental set up. The inset figure in (b) is a top view schematic depicting the geometry of the device and the ribbon wire. The pressure is adjusted by the adjuster in y direction and the device moves in the x direction. (c) A typical output electric pulses of the device as it sliding on the ribbon wire. (d) The electric pulse sequences of repeated scanning in the same area in the same direction at different accelerations. (e) A plot of the pulse peak-to-peak amplitude versus the frequency. (f) The electric pulse sequences of the device during a back-and-forth scanning. The forward and backward scanning are highlighted by yellow and pink background color respectively. Dashed lines denote six perfectly reproduced pulses.

For texture and sliding motion detecting, we used a ribbon wire with relatively large and regular bumpy structure, as shown in Figure 3a, as detecting object. The test set-up is shown in Figure 3b. The ribbon wire was fixed on a manual linear stage, whose position was tuned in y axis so that the ribbon wire had a gentle contact with the device. The device was fixed on a motorized positioning platform, which was programmed to move back-and-forth in x direction. When the device, which had a gentle contact with the ribbon wire, moved in x axis, a sequence of piezoelectric pulse was recorded. A typical result is shown in Figure 3c. During the test, the motorized positioning platform was programmed to accelerate from a full stop

at an acceleration 1 mm/S^2 for 5.4 seconds and then decelerate at a deceleration 1 mm/S^2 for another 5.4 seconds to come to a full stop again. As the device sliding sped up (slowed down) on the ribbon wire, the width of the pulses decreased (increased) and the amplitude of the pulses increased (decreased). The frequency of the electric pulses is decided by the velocity of the sliding device.

The correlation between the pulse width, amplitude and the sliding motion is the basement for sliding motion sensation. For a given surface texture like the period bumpy structure of the ribbon wire, the sliding speed could be calculated from the frequency of the pulses. To verify if the electric pulses faithfully recorded the sliding motion, we calculated the frequency from the width of each pulse and plot it versus time in Figure S1. The acceleration is estimated to be 1.03 mm/S^2 from this plot. This is in a perfect agreement with the setting value (1 mm/S^2) of the acceleration. The calculation detail is given in supporting information. This result confirmed that the electric pulses faithfully recorded the sliding motion. However, in most application, we are not aware of the detecting texture before we start the measurement. This problem could be solved by assembling two devices in parallel with a given distance between them along the scanning direction, then the scanning speed could be calculated from the phase shift of the pulses sequences given by this two devices. To further distinguish the sliding motion in different directions, we may need array of the sensors.

The amplitude of the current is decided by the amount of the charge and how fast it been pumped. The regularity of the bumpy structures defines a similar deformation of artificial finger-print as it scans over each bumpy structure. The total amount of charge driven by the NG beneath the artificial finger-print is presumably the same for each pulse. In this case, the amplitude of the pulses should depend on the scanning speed. To study the relationship between the pulse amplitude and the scanning speed of our device, we programmed the device to scan a 20-mm-area (crossing ~15 wires) at different acceleration (deceleration). The results are shown in Figure 3d. About fifteen pulses have been obtained for each scan. The pulse amplitude increased as the acceleration increased from 5 mm/S^2 to 15 mm/S^2. In Figure 3d, we further plot the amplitude of each pulse in the acceleration stage in Figure 3c versus frequency (1/T), since the frequency (1/T) reflects scanning speed. The plot roughly follows a linear relation. When the device velocity increases, the same amount of charge is pumped in a shorter time and so it gives a higher current. The correlation between the pulse amplitude and the scanning speed may provide a new dimension of sliding motion sensation.

The stability and repeatability of the device performance is very important for the operation. We programmed the automatic linear stage moving back-and-forth so that the device scanned the same area of the ribbon wire repeatedly. The scanning length was 10 mm and the acceleration was set as 30 mm/S^2. The pulse sequences are plotted in Figure 3f. The current pulse sequences show also increasing amplitude and then decreasing amplitude due to the acceleration and the deceleration in spite of some deviations due to the imperfect uniformity of the bumpy structures. However, the very positive message is that the pulse sequences including the pulses with little deviations repeated perfectly for both the forward and backward scanning even in the subtle details (as denoted by the grey and red dashed lines).

To verify the function of the artificial finger-print, a control experiment was carried out with a device without flexible ridge. We used the same test setup with the same strategy. The test results are shown in Figure S2. There is no noticeable electric pulse output. This result confirmed that the artificial finger-print is the key in transferring the mechanic deformation to the NG beneath.

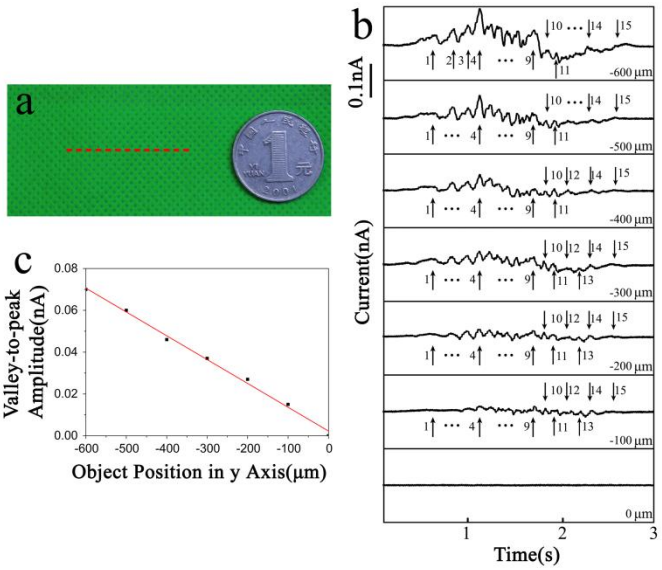

Figure 4. Cloth texture detecting test. (a) Photograph of the nonwoven cloth. Dashed line in (a) shows the scanning path. (b) The output electric pulse sequences of the device in the nonwoven cloth texture detecting test at different contact pressure. From top to bottom, the nonwoven cloth was stepwise moved in y direction with step size 100 μm until it was completely separated from the device after six steps. The pulses are numbered and indicated by arrows. (c) Plot of valley-to-peak amplitude of the 4th pulse in (b) versus the position of the nonwoven cloth in y axis. The position of the detecting object in y axis in the last scan, when the cloth is just detached from the device, is set as zero. The position of the nonwoven cloth in y axis in the 1st scan to the 7th scan is -600 μm, -500 μm, -400 μm, -300 μm, -200 μm, -100 μm and 0, respectively.

The device should be able to detect a finer texture. We further used a piece of nonwoven cloth as testing object. The feature of the nonwoven cloth is that there are array of punch holes with pitch about 2 mm and depth about 200 μm, as shown in Figure 4a. The thickness of the nonwoven cloth is about 800 μm. The scanning area was about 30 mm as indicated by dashed line in Figure 4a. The acceleration and deceleration are both set at 30 mm/S^2 for the starting and stopping stage. The pressure between the device and the nonwoven cloth was adjusted by the manual linear stage in y axis, as shown in Figure 3b. The position of the nonwoven cloth in y axis defines the pressure between the device and the nonwoven cloth. The test started from a tight contact position and then the device was stepwise released from the cloth for each scan.

The test results of the nonwoven cloth texture detecting are shown in Figure 4b. Fifteen pulses can be identified in the output signal of the scans except the last one, where the nonwoven cloth is already detached from the device. The electric pulses are numbered and indicated by arrows. The fifteen electric pulses in the scans are responses of the device to the 15 punch holes along the scanning path. The very positive message of the result is that those pulses are well reproduced even in some details at different pressure status. For example, the 4th pulse shows the highest amplitude while the 11th to 13th pulses are significantly lower in amplitude. The pulses in all of the scans (except the last one) overlap perfectly in time axis. This

result indicates that our device is capable of capturing the texture feature of the nonwoven cloth in a large range of pressure. This capability is very important because in real application we can hardly define the pressure status precisely. The reproduction of the pulse sequences at different pressure status ensures that the sensor can give a similar texture judgement no matter it is in a gentle or a tight contact with the object. At this stage, to rebuild the exactly shape change from the current amplitude change is impossible since the current amplitude depends on multiple factors: the shape of texture, the scanning speed as well as the contact distance.

To study the relationship between the signal strength (pulse amplitude) and the pressure status, the valley-to-peak amplitude of the 4th pulse versus the position of nonwoven cloth in y axis is plotted in Figure 4c, since the position of the object defines the pressure between the device and the object. Roughly, the valley-to-peak amplitude of the pulse decrease linearly with the y position of the nonwoven cloth. In the last scan, the device was completely detached from the cloth and it gives no output signal. The amplitude of most of the pulses decreases consistently as the nonwoven cloth being stepwise released from the device.

The NG-type tactile sensor reported here demonstrates a reliable responds to the texture and sliding motion. This is the physical base towards tactile sensation with our device. However, how to translate the pulses sequences into tactile information still remains an open question. To obtain the relationship between the electric pulses (in terms of pulse width, amplitude and polarity) and the texture and sliding motion is the first step. The results of the test with ribbon wire and nonwoven cloth reveal two basic correlations between the pulses and the texture and sliding motion: 1. the pulse width is determined by the scanning speed and the pitch of the textured surface; 2. the pulse amplitude is determined by both the pressure and the scanning speed.

Because the NG-type tactile sensor has only a single sensitive unit, the spatial resolution is decided by the pulse resolution in time axis. In the nonwoven cloth test, 15 pulses have been recorded within a ~2 second duration scanning. The average pulse width is about 130 ms in corresponding to a 2 mm pitch of punch holes. How fast the current in external circuit follows the strain events is decided by both the impedance of the driven circuit and the resonance frequency of the artificial finger-print. There should be plenty of room for improvement. The depth of the punch hole is 200 μm. It indicates a sub-millimetre sensitivity of our device to the bumpy structures. The spatial resolution of tactile sensor has been set a record down to 2.7 μm by Pan et al with array of ZnO nanowire grown on p-GaN film[11]. The NG-type tactile sensor may not be able to reach that high spatial resolution. However, the successful detecting of the texture feature of a nonwoven cloth verified its competence for some simple texture and sliding motion recognition missions.

The SGVPT based tactile sensor[10] is a milestone work in the field of tactile sensors. Its spatial resolution has reached 234 taxels per inch. It comprises 92× 92 sensitive units and its sensitivity have reached 2.1 S Pa^{-1}. The SGVPT based tactile sensor is an integrated piezotronic device, which has demonstrated promising applications in human-electronics interfacing, smart skin, and micro- and nanoelectromechanical systems. The NG-type tactile sensor reported here is a single device based on previous nanowire device. The unique feature of the device structure lays in the artificial finger print, which changes the strain direction. The artificial finger print allows the active sensor, a ZnO based nanogenerator, to sense external stress, besides tension/compressive stress or bend the device directly. The performance of the device is highly depends on the nanogenerator beneath the artificial finger print.

Most of the performances of the NG-type tactile sensor cannot compete with the SGVPT based tactile sensor. However, with active signal output and demand for small number of devices, the NG-type tactile sensor might be a complementary technique for those highly advanced pressure image capturing tactile sensors. For example, the NG-type tactile sensor may serve an awakening unit for the SGVPT tactile sensor. When a sequence of piezoelectric pulses have been recorded, it could provide a rough judgment if the object is of interest and decide whether the SVGPT tactile sensor should be awaked to capture detailed texture information to provide a keen tactile sensation. The NG-type tactile sensor alone might be also applicable for some simple tactile recognition jobs, such as identifying several given objects with identical different texture features.

Conclusions

In summary, we present a NG-type tactile sensor, which demonstrate a capability of recording the fine texture of nonwoven cloth. In a ribbon wire texture detecting experiment, the acceleration of the sliding motion is precisely detracted from the width of the electric pulses with error less than 3%. It indicates that the device faithfully records the sliding motion as well. In a back-and-forth sliding motion on the ribbon wire, the device reproduced the electric pulses perfectly for both the forward and backward scanning. In a test with nonwoven cloth, the electric pulses of the device recorded all of the punch holes on the cloth in the scanning path in a large range of pressure status. The shape of electric pulses is well reproduced. The NG-type tactile sensor reported here provides a new approach for tactile sensation. Other than pressure image capturing, the NG-type tactile sensor translate the texture and sliding motion information into sequence of electric pulses. The texture and sliding motion information is conveyed by the amplitude, the width and the polarity of the piezoelectric pulses. The simple working mechanism of the NG-type tactile sensor asks for a much simple driven circuit and it don't need power input from the driven circuit during its operation. How to interpret the electric pulses into meaningful tactile information will be an interesting topic in the future. The NG-type tactile sensor might serve as a supplementary technology for those pressure image capturing tactile sensors.

Acknowledgements

This work was financially supported by the National Natural Science Foundation of China (Grant Nos. 61172041, 61172040, 11375139, 91123018 and 60801022) and the Fundamental Research Funds for the Central Universities. The authors thank Prof. Yong Qin for providing high quality ZnO micro/nanowires.

Notes and references

[a] Department of Microelectronics, School of Electronics and Information Engineering, Xi'an Jiaotong University, Xi'an 710049, China. E-mail: lwhua@mail.xjtu.edu.cn; Tel: +86 29-8266-3343.

[b] Beijing Institute of Nanoenergy and Nanosystems, Chinese Academy of Sciences, Beijing 100083, China;

[c]Institute of Theoretical Physics, and Key Laboratory for Magnetism and Magnetic Materials of MOE, Lanzhou University, Lanzhou 730000, China

‡ Electronic Supplementary Information (ESI) available: [details of any supplementary information available should be included here]. See DOI: 10.1039/b000000x/

1 (a) Z. L. Wang, *Mat Sci Eng R*, **2009,** *64* (3-4), 33; (b) Z. L. Wang, R. S. Yang, J. Zhou, Y. Qin, C. Xu, Y. F. Hu and S. Xu, *Mat Sci Eng R*, **2010,** *70* (3-6), 320; (c) Z. L. Wang and J. H. Song, *Science*, **2006,** *312* (5771), 242; (d) Z. L. Wang, *Acs Nano*, **2013,** *7* (11), 9533; (e) F. R. Fan, Z. Q. Tian and Z. L. Wang, *Nano Energy*, **2012,** *1* (2), 328.

2 F. R. Fan, L. Lin, G. Zhu, W. Wu, R. Zhang and Z. L. Wang, *Nano Lett*, **2012,** *12* (6), 3109.

3 (a) S. Xu, Y. Qin, C. Xu, Y. G. Wei, R. S. Yang and Z. L. Wang, *Nat Nanotechnol*, **2010,** *5* (5), 366; (b) Y. Qin, X. D. Wang and Z. L. Wang, *Nature*, **2008,** *451* (7180), 809; (c) J. W. Zhong, Y. Zhang, Q. Z. Zhong, Q. Y. Hu, B. Hu, Z. L. Wang and J. Zhou, *Acs Nano*, **2014,** *8* (6), 6273; (d) Y. J. Su, X. N. Wen, G. Zhu, J. Yang, J. Chen, P. Bai, Z. M. Wu, Y. D. Jiang and Z. L. Wang, *Nano Energy*, **2014,** *9*, 186; (e) Y. N. Xie, S. H. Wang, S. M. Niu, L. Lin, Q. S. Jing, Y. J. Su, Z. Y. Wu and Z. L. Wang, *Nano Energy*, **2014,** *6*, 129.

4 (a) A. F. Yu, Y. Zhao, P. Jiang and Z. L. Wang, *Nanotechnology*, **2013,** *24* (5); (b) C. B. Han, C. Zhang, X. H. Li, L. M. Zhang, T. Zhou, W. G. Hu and Z. L. Wang, *Nano Energy*, **2014,** *9*, 325; (c) Y. S. Zhou, G. Zhu, S. M. Niu, Y. Liu, P. S. Bai, Q. Jing and Z. L. Wang, *Adv Mater*, **2014,** *26* (11), 1719.

5 F. McGlone and D. Reilly, *Neurosci Biobehav R*, **2010,** *34* (2), 148.

6 (a) S. C. B. Mannsfeld, B. C. K. Tee, R. M. Stoltenberg, C. V. H. H. Chen, S. Barman, B. V. O. Muir, A. N. Sokolov, C. Reese and Z. N. Bao, *Nat Mater*, **2010,** *9* (10), 859; (b) H. K. Kim, S. Lee and K. S. Yun, *Sensor Actuat a-Phys*, **2011,** *165* (1), 2; (c) H. B. Muhammad, C. M. Oddo, L. Beccai, C. Recchiuto, C. J. Anthony, M. J. Adams, M. C. Carrozza, D. W. L. Hukins and M. C. L. Ward, *Sensor Actuat a-Phys*, **2011,** *165* (2), 221.

7 (a) K. Takei, T. Takahashi, J. C. Ho, H. Ko, A. G. Gillies, P. W. Leu, R. S. Fearing and A. Javey, *Nat Mater*, **2010,** *9* (10), 821; (b) M. Shimojo, A. Namiki, M. Ishikawa, R. Makino and K. Mabuchi, *Ieee Sens J*, **2004,** *4* (5), 589; (c) M. Hussain, Y. H. Choa and K. Niihara, *J Mater Sci Lett*, **2001,** *20* (6), 525. (d) B. W. Zhu, Z. Q. Niu, H. Wang, W. R. Leow, H. Wang, Y. G. Li, L. Y. Zheng, J. Wei, F. W. Huo and X. D. Chen, *Small*, **2014,** *10* (18), 3625; (e) Q. Shao, Z. Q. Niu, M. Hirtz, L. Jiang, Y. J. Liu, Z. H. Wang and X. D. Chen, *Small*, **2014,** *10* (8), 1466.

8 (a) C. Y. Li, P. M. Wu, S. Lee, A. Gorton, M. J. Schulz and C. H. Ahn, *J Microelectromech S*, **2008,** *17* (2), 334; (b) A. V. Shirinov and W. K. Schomburg, *Sensors and Actuators A: Physical*, **2008,** *142* (1), 48.

9 (a) Z. L. Wang, *J Phys Chem Lett*, **2010,** *1* (9), 1388; (b) J. Zhou, Y. D. Gu, P. Fei, W. J. Mai, Y. F. Gao, R. S. Yang, G. Bao and Z. L. Wang, *Nano Letters*, **2008,** *8* (9), 3035; (c) X. Xiao, L. Y. Yuan, J. W. Zhong, T. P. Ding, Y. Liu, Z. X. Cai, Y. G. Rong, H. W. Han, J. Zhou and Z. L. Wang, *Adv Mater*, **2011,** *23* (45), 5440; (d) Y. Zhang, Y. Liu and Z. L. Wang, *Adv Mater*, **2011,** *23* (27), 3004; (e) W. Z. Wu, C. F. Pan, Y. Zhang, X. N. Wen and Z. L. Wang, *Nano Today*, **2013,** *8* (6), 619.

10 W. Wu, X. Wen and Z. Wang, *Science (New York, N.Y.)*, **2013,** *340* (6135), 952.

11 C. F. Pan, L. Dong, G. Zhu, S. M. Niu, R. M. Yu, Q. Yang, Y. Liu and Z. L. Wang, *Nat Photonics*, **2013,** *7* (9), 752.

12 K. O. Johnson, *Current Opinion in Neurobiology*, **2001,** *11* (4), 455.

13 H. K. Lee, S. I. Chang and E. Yoon, *J Microelectromech S*, **2006,** *15* (6), 1681.

14 R. S. Yang, Y. Qin, L. M. Dai and Z. L. Wang, Nat Nanotechnol, 2009, 4 (1), 34.

